Proceedings of the Thirty-fourth (2024) International Ocean and Polar Engineering Conference **www.isope.org**
Rhodes, Greece, June 16–21, 2024

ISBN 978-1-880653-78-4; ISSN 1098-6189

Grid Resolution Requirements for Wall-Resolved Large Eddy Simulation of Wall Pressure Fluctuations in Turbulent Channel Flows

Yihang He[1], Fuchang Zhou[2], Weiwen Zhao[1], Decheng Wan[1]*

[1] Computational Marine Hydrodynamics Lab (CMHL), School of Naval Architecture, Ocean and Civil Engineering, Shanghai Jiao Tong University, Shanghai, China
[2] Wuhan Second Ship Design and Research Institute, Wuhan, China

[*]Corresponding Author

ABSTRACT

Large eddy simulation (LES) of incompressible channel flow at friction Reynolds number of Re_τ = 1000 are conducted to investigate the wavenumber-frequency spectrum of turbulent wall pressure fluctuations. To assess the minimal cost of LES for accurately capturing wall-pressure fluctuations, various grid resolutions in both streamwise and spanwise directions in the boundary layer are investigated. All simulations were conducted using OpenFOAM, a computational fluid dynamics software package. The mean velocity profiles, turbulence intensities, and wavenumber-frequency spectrum obtained from different grid resolution are compared with other computational and experimental results. It is demonstrated that logarithmic layer mismatch (LLM) is observed in coarse spanwise grid resolution where the wall-shear stress deviates from the true data. On the other hand, coarse streamwise grid resolution can capture time-averaged quantities well, but for the wall pressure fluctuations, the higher grid resolution requirement is essential. Our analyses indicate that the wall pressure fluctuations are sensitive to the grid resolution, the near-wall, short-time and small-scale eddies need to be resolved for accurate prediction of the wall-pressure fluctuations.

KEY WORDS: Large eddy simulation; grid resolution; wall pressure fluctuation; wavenumber-frequency spectrum.

INTRODUCTION

Large Eddy Simulation (LES) method is a computational fluid dynamics (CFD) method that directly resolves the large-scale motions ("large eddies") while modeling the small-scale motions. In this method, approximately 80% of the energy-containing eddy structures are resolved, and the remaining small eddies are modeled using sub grid scale models. However, when the LES method encounters situations with wall-bounded flows, the eddy structures near the wall are constrained which results in the existence of numerous small-scale eddy structures containing significant energy near the wall. To effectively employ WRLES for resolving near-wall eddy structures, an extremely fine grid resolution is required near the wall. Although Wall-Modeled Large Eddy Simulation (WMLES) methods can reduce the computational grid requirements, further research and analysis are needed to simulate wall-pressure fluctuations accurately. Hence, the grid resolution for wall-resolved Large Eddy Simulation (WRLES) to accurately simulate wall-pressure fluctuations at minimal cost is discussed in this paper.

The first formal estimate for the grid-point requirement for LES is conducted by Chapman (1979). He proposed grid resolution requirements for LES based on the relationship between the skin friction coefficient and Reynolds number within the boundary layer combined with the seventh-power velocity distribution law. According to his calculations, the grid point requirements for WMLES and WRLES is $N \sim Re_L^{2/5}$, $N \sim Re_L^{7/5}$, respectively. where N is the number of grid points and L represents the characteristic length scale. However, the requirements he proposed is only effective for $Re<10^6$. Building upon Chapman's work, Choi and Moin (2012) proposed new grid point requirements for WMLES, WRLES and DNS by utilizing more accurate boundary layer flow formulations in high Reynolds number. The grid point requirements for WMLES, WRLES and DNS require $N \sim Re_L$, $N \sim Re_L^{13/7}$ and $N \sim Re_L^{37/14}$, respectively. Based on these foundations, Yang (2021) reevaluated the grid point requirements for spatially developing turbulent boundary layers in DNS, WRLES, and WMLES. Additionally, he estimated the time step requirements for different numerical computation methods. By combining the grid point requirements with the time step requirements, the estimated costs for DNS, WRLES, and WMLES are $N \sim Re_L^{2.91}$, $N \sim Re_L^{2.72}$, and $N \sim Re_L^{1.14}$, respectively. The methods mentioned above for estimating the number of grid points are based on the entire computational domain. For local grid scales near the wall boundary layer, Chapman (1979), Moin (1996), and Chung (2010), recommend Δx^+ =50~100, Δz^+ =15~30 for WRLES. Where superscript + represents non-dimensionalized by using the wall units ν / μ_τ as characteristic length. Rezaeiravesh (2018) investigated the effect of grid resolution on a large eddy simulation of wall-bounded turbulence at Re_τ =300, evaluated the error responses between the LES results including the wall mean friction velocity and

the cross-channel profiles of mean velocity and Reynolds stress components with DNS data. Based on these evaluations, grid ranges for these variables were recommend as Δx^+ =10~45, Δz^+ =7~30. However, their grid point estimations are designed specifically for time-averaged values. When calculating wall pressure fluctuations, a more refined grid resolution is necessary to fulfill the requirements for precise predictions.

Wall pressure fluctuations serve as the predominant origins of flow-generated noise in wall-bounded turbulence flows (Kravchenko et al,.1996; Chung et al,.2010). Based on the CFD approach, many scholars have established a series of spectral analysis methods to investigate the characteristics of wall pressure fluctuations. Kim (1989) pioneered the investigation of wall pressure fluctuations in turbulent channel flow at Re_τ = 180 through DNS. The investigation specifically delved into aspects such as root mean square (r.m.s.) profiles, one-dimensional spectra (both in wavenumber and frequency), and probability density functions. Anantharamu and Mahesh (2020) proposed that the primary source of wall-pressure fluctuations originates in the buffer layer. Namely, in the region where $y+$ is greater than 5 and less than 30. Hu(2006) analyzed DNS data of turbulent channel flow at Re_τ = 90 ~ 1440. The study focused on the scaling behavior of wall-pressure fluctuation spectra at different characteristic frequencies. Yang (2022) utilized spectral analysis methods to analysis wall pressure fluctuations. He conducted Direct Numerical Simulations (DNS) of turbulent channel flow at different Re_τ up to 1000. The study focused on the three-dimensional spectrum of wall pressure fluctuations, consisting of streamwise wavenumber, spanwise wavenumber, and frequency. Additionally, he investigated the time decorrelation mechanisms of wall pressure fluctuations. Francis (2023) analyzed the temporal evolution of wall-pressure fluctuations, this study aims to estimate the wall pressure fluctuation spectrum. In this process, comprehensive estimations were made for the convective ridge as well as the sub-convective and low-wavenumber components of the spectrum.

In the present study, WRLES for channel flow at Re_τ =1000 is presented. The primary objectives are to analyze the grid resolution requirements for time-averaged quantities and wall pressure fluctuations in WRLES. This paper is organized as follows. First, the numerical methods are introduced in detail, including governing equations and sub-grid scale (SGS) stress model. Then, the numerical setup for WRLES is presented. Following this, comparisons were presented between WRLES with different streamwise and spanwise grid resolutions and the corresponding results obtained from DNS. Finally, the conclusions of the present study are reported.

NUMERICAL METHODS

In LES, only the large energy-containing eddies are accurately computed. Small-scale eddies are not precisely computed, but their impact on the flow field is numerically simulated. By applying a filter to the incompressible N-S equation, the governing equations can be written as

$$\frac{\partial \tilde{u}_i}{\partial x_i} = 0, \tag{1}$$

$$\frac{\partial \tilde{u}_i}{\partial t} + \frac{\partial \tilde{u}_i \tilde{u}_j}{\partial x_j} = -\frac{1}{\rho}\frac{\partial \tilde{p}}{\partial x_i} + \nu \frac{\partial^2 \tilde{u}_i}{\partial x_j \partial x_j} - \frac{\partial \tau_{ij}}{\partial x_j}, \tag{2}$$

Where $\tilde{u}_i$ (i =1, 2, and 3) is the filtered velocity component, $\tilde{p}$ is the filtered pressure, ν is the kinematic viscosity of the fluid, and τ_{ij} is the SGS stress term, which can be written as

$$\tau_{ij} = \frac{2}{3} k_{sgs} \delta_{ij} - 2\nu_{sgs} \tilde{S}_{ij}, \tag{3}$$

where k_{sgs} is the SGS kinetic energy, δ_{ij} is the Kronecker delta, ν_{sgs} is the SGS eddy viscosity, and $\tilde{S}_{ij}$ is the resolved strain-rate tensor. In this paper, the wall-adapting local eddy-viscosity (WALE) model (Nicoud & Ducros 1999) is utilized. The SGS eddy viscosity is obtained by

$$\nu_{sgs} = (C_w \Delta)^2 \frac{(S_{ij}^d S_{ij}^d)^{3/2}}{(\tilde{S}_{ij}\tilde{S}_{ij})^{5/2} + (S_{ij}^d S_{ij}^d)^{5/4}} \tag{4}$$

where C_w =0.325 is the WALE coefficient, S_{ij}^d is the traceless symmetric part of the square of the velocity gradient tensor.

NUMERICAL SETUP

The focus of the present study is to validate and analyze turbulent channel flow simulations at various grid resolutions by comparing them with the DNS results obtained by Yang (2022) at Re_τ =1000. The DNS were conducted for turbulent channel flow with the main dimensions of 12.56h × 2h × 6.28h (length × width × depth), where 'h' represents half height of channel. All simulations were conducted using OpenFOAM, a computational fluid dynamics software package.

Computational domain and mesh

To save computational costs, the simulations utilized a computational domain for turbulent channel flow with dimensions of 6.28h × 2h × 3.14h. This study investigated impacts of various streamwise and spanwise grid resolutions to mean statistics and wall pressure fluctuations. Detailed grid information is provided in Table 1. The detailed grid information of Case 1 is depicted in Fig 1. The grids are uniformly distributed in the streamwise and spanwise. Along the wall-normal direction, the grid resolution varies proportionally with the distance from the wall, and the expansion ratio is set to 1.05.

Table 1. Computational cases

Case	Δx^+ , Δy^+ , Δz^+	Total cells number
1	15 , 1 , 15	9,878,400
2	20 , 1 , 15	7,409,550
3	30 , 1 , 15	4,939,700
4	50 , 1 , 15	2,963,820
5	15 , 1 , 10	14,817,600
6	15 , 1 , 20	7,409,550
7	15 , 1 , 30	4,939,700
8	15 , 1 , 50	2,963,820

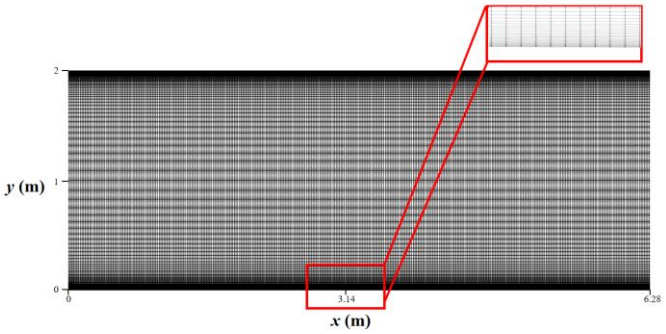

Fig. 1. Computational mesh. (Case 1)

Boundary and initial conditions

Periodic boundary conditions are applied in the streamwise and spanwise, while no-slip conditions are set for the solid walls. The flow is driven by a streamwise pressure gradient, and the pressure gradient is adjusted to maintain a constant mean velocity in the computational domain. In order to obtain the wavenumber–frequency spectra of turbulent wall pressure fluctuations in the time domain, a series of pressure sensors have distributed evenly along the streamwise direction at the bottom of the turbulent channel (y=0, z=1.57h). To save the time for the development of the velocity field, initial velocity perturbations are imparted to expedite the transition from laminar to fully developed turbulent flow (Villiers, 2006). For the present study, a second-order linear scheme is used to discretized the convection terms, as for time integration, an implicit second-order backward scheme is used. PISO algorithm is used to solve the coupled pressure–velocity equation. The time step is set as 0.01s to ensure that the maximum Courant number is less than 0.5. All simulations are performed for a duration exceeding 15 dimensionless time units (tu_τ / h) after the physical quantities reach a quasi-stationary state to ensure sufficient periods for obtaining stable statistics for subsequent analysis.

RESULTS AND DISCUSSION

In this section, the results of different grid resolution of streamwise and spanwise will be presented. Both the time-averaged properties and the spectrum of wall pressure fluctuations will be analyzed.

Mean flow statistics

The time-averaged properties are analyzed prior to the recording of pressure data at the monitoring points. Table 2 shows the average variables of turbulent channel flow under different cases. The theoretical values are calculated by $C_f = \tau_w / 0.5\rho U^2$ and $U_c / U_0 = 1.28\,\mathrm{Re}^{-0.0116}$ proposed by Dean (1978), where U_c is the velocity of centerline of the channel. It can be observed that the actual computed values are consistently smaller than the values predicted by empirical formulas, with minimal influence from changes in the streamwise grid, but significant influence are observed in the spanwise direction. The mean velocity profiles of different streamwise and spanwise grid resolution along the wall-normal directions are presented in Fig. 2 and Fig. 3 respectively. The mean velocity has been averaged both temporally and spatially. Spatial averaging is performed within the X-Z plane. The mean velocity and the distance away from the wall are both nondimensionalized by the friction velocity and the molecular viscosity, which can be written as $u^+ = u / u_\tau$, $y^+ = y u_\tau / \mu$, respectively. The friction velocity $u_\tau = \sqrt{\tau_w / \rho}$, where τ_w represents the mean wall shear stress. Note that in Fig.2, expanding the streamwise grid resolution while maintaining grid resolution in the spanwise has a negligible impact on the mean velocity profile. All cases have good agreement with both the logarithmic law $U^+ = \log y^+ / \kappa + B$,where κ =0.4 and B=5.5 are constants (Bailey, 2014) and DNS results (Yang, 2022) in the viscous sublayer and the logarithmic layer. However, in Fig.3, changing the spanwise grid resolution has a significant impact on the results. The calculation results are favorable only when $\Delta z^+ \leq 15$. While alterations to the streamwise grid resolution have minimal effects on the computed results in the viscous sublayer, having favorable agreement with the reference data, as y^+ increases, the LLM phenomenon occurs with the coarser grid resolution in the logarithmic region, which is mainly caused by error in the wall friction velocity. As the wall friction velocity decreases, the amplitude of the mean velocity profile in the logarithmic region is significantly elevated, ultimately leading to the LLM phenomenon.

Table 2. Mean flow statistics

Case	C_f	U_c / U_0
Theoretical value	0.00500	1.1410
1	0.00470	1.1369
2	0.00465	1.1331
3	0.00459	1.1315
4	0.00456	1.1281
5	0.00476	1.1382
6	0.00437	1.1217
7	0.00396	1.1181
8	0.00318	1.1184

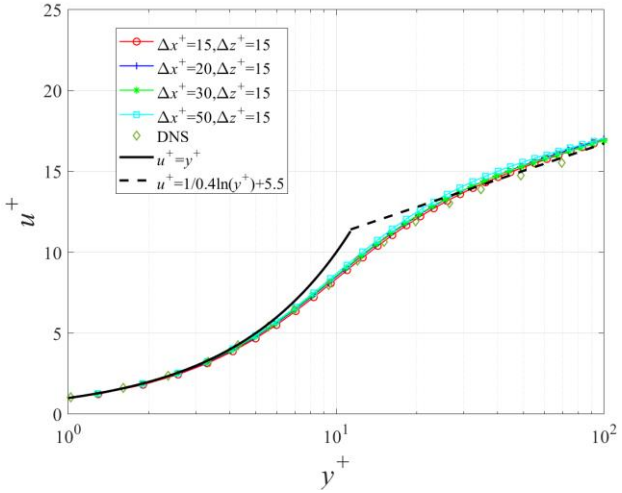

Fig. 2. Mean velocity profile of different streamwise grid resolution.

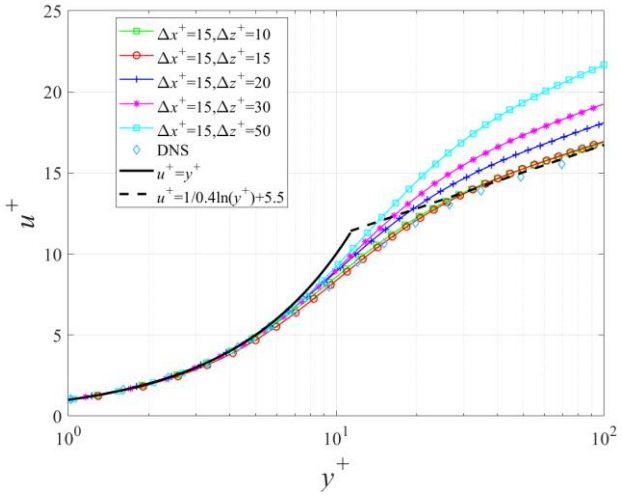

Fig. 3. Mean velocity profile of different spanwise grid resolution.

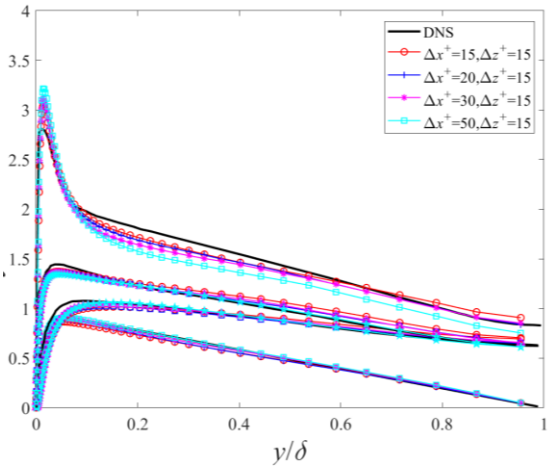

(a)

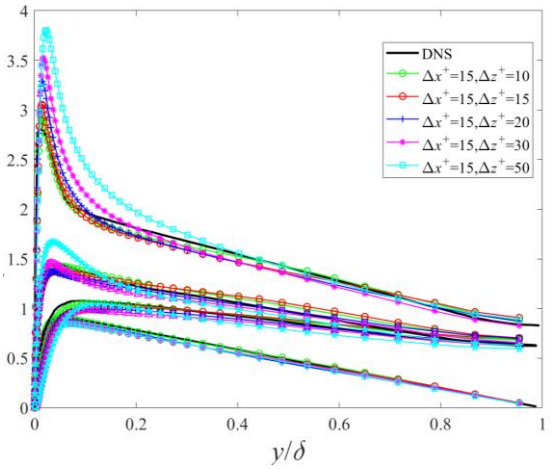

(b)

Fig. 4. Profiles of root mean square of velocity fluctuations and SGS shear stress (superscript + represents non-dimensionalized by friction velocity u_τ). (a) different streamwise grid resolution, (b) different spanwise grid resolution.

The impact of the grid resolution on the root mean square (rms) values of streamwise, wall-normal, spanwise velocity fluctuations and the SGS shear stress are illustrated in Fig. 4. Additionally, comparative data from DNS (Lee & Moser, 2015) is provided for reference. Fig. 4(a) and Figure 4(b) show root mean square of velocity fluctuations of different streamwise and spanwise grid resolution, respectively. As for streamwise grid resolution, the wall-normal and spanwise velocity fluctuations are observed similar results for the four different streamwise grid resolution. For the streamwise velocity fluctuations, there is a significant difference in peak values among the four streamwise grid resolution, with larger grid scales yielding higher predicted peaks and greater deviations from DNS results. For coarse spanwise grid resolution, not only are the peak values in the streamwise direction overestimated, but the peak values in the spanwise direction are also subject to overestimation, and the magnitude of this overestimation is even more substantial. As for the SGS shear stress, all cases align well with the DNS results. In general, an insufficient streamwise grid resolution can lead to an overestimation of streamwise velocity fluctuations, on the other hand, an insufficient spanwise grid resolution can lead to an exaggerated overprediction for both streamwise and spanwise velocity fluctuations.

Wall pressure fluctuation

The current analysis of turbulent wall pressure fluctuations primarily relies on Fourier analysis to achieve the transformation between the time-space and wavenumber-frequency domains. This allows for the investigation of statistical characteristics of signals in the wavenumber-frequency domain. The wavenumber-frequency spectrum of wall pressure fluctuations is then calculated as

$$\phi(\vec{k},\omega)=\int_{-\infty}^{+\infty}R(\vec{\xi},\tau)e^{-(\vec{k}\cdot\vec{\xi}+\omega\tau)}d\vec{\xi}\,d\tau, \tag{5}$$

Since all the LES data are calculated on discrete grids, in the present study, the wavenumber-frequency spectrum is obtained through Fast Fourier Transform (FFT) of the discretized signal of turbulent pressure fluctuations. Subsequently, ensemble averaging of the square of its amplitude is performed to obtain the wavenumber-frequency spectrum as

$$\phi_{pp}(k,\omega)=\frac{\left|\sum_{n=1}^{N}\sum_{m=1}^{M}W(x_m,t_n)\,p_m(x_m,t_n)e^{-i(k_x x_m+\omega t_n)}\Delta x\Delta t\right|^2}{(2\pi)^2 NMC_w}, \tag{6}$$

where p_m represents the pressure measured at the wall pressure sensor, Δx represents the spacing between measurement points, and Δt represents the time step. N represents the total sampling time, M represents the number of wall pressure sensors, $W(x_m, t_n)$ is the window function, and in this paper, the Hanning window is chosen. C_w is defined as follows:

$$C_w=\frac{\sum_{n=1}^{N}\sum_{m=1}^{M}W^2(x_m,t_n)}{NM}, \tag{7}$$

The pressure spectrum in the frequency domain of single point of the turbulent boundary layer wall pressure fluctuations, $\Phi_{pp}(\omega)$, is obtained from the wavenumber–frequency spectrum, $\Phi_{pp}(k,\omega)$ by using

$$\Phi_{pp}(w)=\int_{-\infty}^{\infty}\Phi_{pp}(k,w)dk, \tag{8}$$

Fig. 5 shows the one-dimensional frequency spectra of turbulent boundary layer wall pressure fluctuations of the four streamwise grid resolutions, obtained from the present LES and non-dimensionalized with inner variables, $\Phi_{pp}(\omega)u_\tau^2/\tau_w\nu$. The dimensionless spectra are compared with DNS data (Yang, 2022). At small frequencies, the magnitudes of one-dimensional spectra of all streamwise grid resolution agrees well with the DNS results. However, in the high frequency region, as the grid resolution becomes coarser, the frequencies where its amplitude starts to decay occur smaller, and the decay rate is faster. This leads to significant mismatches between the LES and DNS results in high frequency region. Moreover, with grids goes coarser, the cutoff frequency which refers to the upper limit frequency of the vortical scales considered in the simulation goes earlier, resulting in reduced confidence in the calculated amplitude of the spectrum in the high-frequency region.

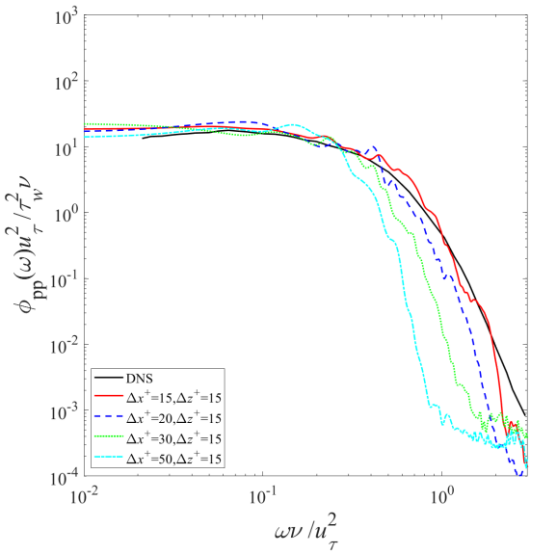

Fig. 5. One-dimensional frequency spectra of wall pressure fluctuations of different streamwise grid resolution. Spectra are non-dimensionalized using inner variables. The DNS results of Yang (2022) are shown for comparison.

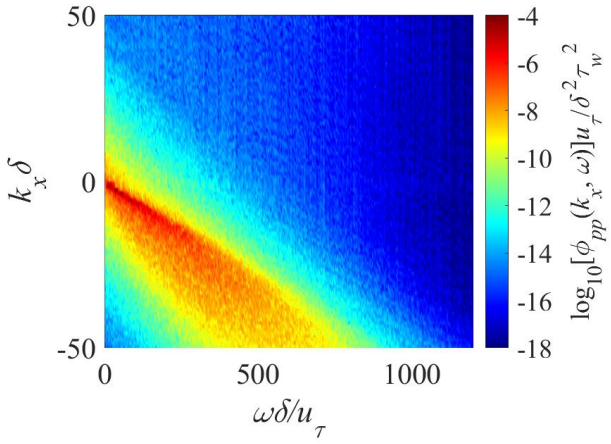

(a)

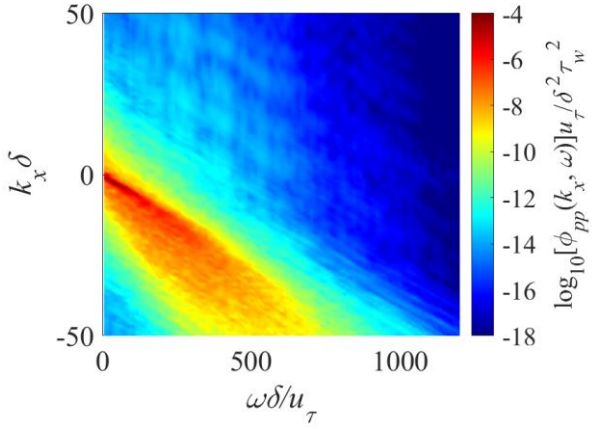

(b)

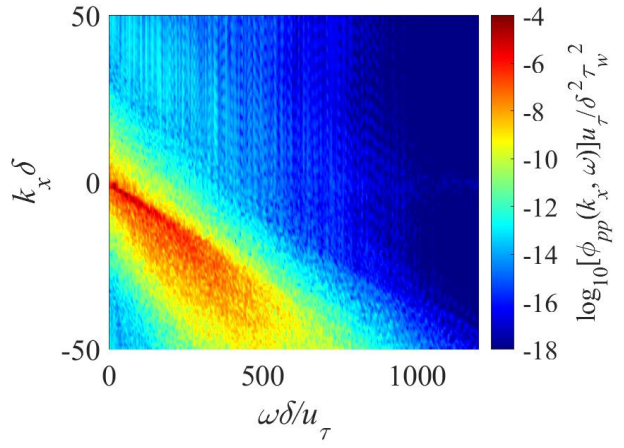

(c)

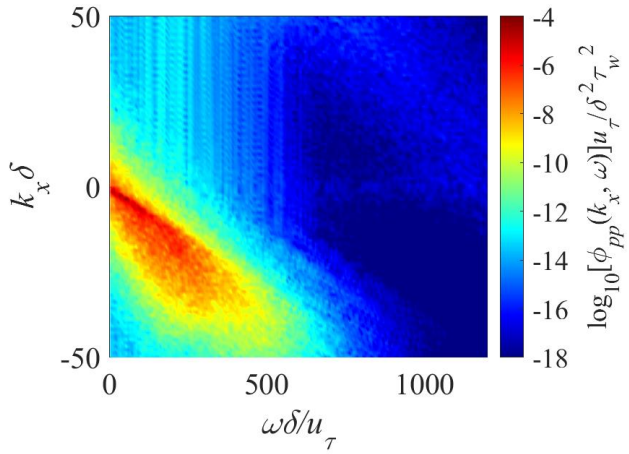

(d)

Fig. 6. Two-dimensional wavenumber-frequency spectra of wall pressure fluctuations of different streamwise grid resolution. (a) Δx^+ =15, (b) Δx^+ =20, (c) Δx^+ =30, and (d) Δx^+ =50. Spectra are non-dimensionalized using inner variables.

The wavenumber-frequency spectra offer spatial and temporal features of wall pressure fluctuations in turbulent boundary layer which can be an input to the analysis of radiated noise. In the wavenumber-frequency spectra, most of the spectral power is concentrated in the region of convective ridge, and the slope of the convective ridge is called convection velocity. Fig. 6 shows the two-dimensional wavenumber-frequency spectra of wall pressure fluctuations of four different streamwise grid resolutions. As the streamwise grid resolution becomes coarser, the amplitude of the wavenumber-frequency spectrum in the convective ridge region decreases. This is due to the inability of the grid resolution in the streamwise direction to resolve high-frequency and high-wavenumber structures, leading to the underestimation of the amplitude of the wavenumber-frequency spectrum.

CONCLUSIONS

In this paper, large eddy simulation was carried out for the turbulent channel flow at Re_τ = 1000 to study the impact of various grid resolutions to wavenumber–frequency spectrum of wall pressure fluctuations. The present numerical results are compared with DNS data,

and analyzed the effect of different grid resolutions by comparing the results of mean flow statistics and spectra of wall pressure fluctuations. Several conclusions are discussed below.

The mean velocity profile is insensitive to the streamwise grid resolution, but for spanwise, coarse grid resolution result in a significant discrepancy between the calculated and actual values of wall shear stress, and ultimately leading to the logarithmic layer mismatch (LLM). For the velocity fluctuations, coarse streamwise grid resolution will cause exaggerated peak values of streamwise velocity fluctuations, while coarse spanwise grid resolution will lead to more exaggerated peak values of both streamwise and spanwise velocity fluctuations. For the spectrum of wall pressure fluctuations, due to significant discrepancies in time-averaged quantities of insufficient spanwise grid resolution, only the effects of streamwise are analyzed. In one-dimensional frequency spectra, coarse streamwise grid resolution will result in premature amplitude decay and an earlier cutoff frequency, leading to significant discrepancies between the predicted and actual results in the high-frequency region. Besides, in two-dimensional wavenumber-frequency spectra, coarse streamwise grid resolution will lead to a decreasing of the amplitude of the wavenumber-frequency spectrum in the convective ridge region, which indicates a poor capture of high-frequency and high-wavenumber fluctuations.

As a final remark in this paper, we note that it is essential to ensure that $\Delta z^+ \leq 15$ to obtain accurate flow properties. For streamwise, $\Delta x^+ = 50$ is enough for time-averaged statistics, but for wall pressure fluctuations, $\Delta x^+ = 15$ is essential to ensure the near-wall, short-time and small-scale eddies are resolved for accurate prediction.

ACKNOWLEDGMENTS

This work is supported by the National Natural Science Foundation of China (52131102), to which the authors are most grateful.

REFERENCES

Anantharamu, S, and Mahesh, K (2020). "Analysis of wall-pressure fluctuation sources from direct numerical simulation of turbulent channel flow," *Journal of Fluid Mechanics*, 898, A17.

Bailey, SV, Allikivi, MH, Ultmark, M, and Smits, AJ. (2014) "Estimating the value of von Kármán's constant in turbulent pipe flow," *Journal of Fluid Mechanics*. 749, 79–98.

Chapman, DR (1979). "Computational aerodynamics development and outlook," *AIAA J*. 17.

Chung, D, and McKeon, BJ (2010). "Large-eddy simulation of large-scale structures in long channel flow," *Journal of Fluid Mechanics*, 661, 341–364.

Choi, H, and Moin, P (1990). "On the space-time characteristics of wall-pressure fluctuations," *Physics of Fluids A: Fluid Dynamics*, 2(8), 1450–1460.

Choi, H, and Moin, P (2012). "Grid-point requirements for large eddy simulation: Chapman's estimates revisited," *Physics of Fluids*, 24.

Cohen, E, and Gloerfelt, X (2018). "Influence of pressure gradients on wall pressure beneath a turbulent boundary layer," *Journal of Fluid Mechanics*, 838, 715–758.

Dean, RB (1978). "Reynolds number dependence of skin friction and other bulk flow variables in two-dimensional rectangular duct flow," *Journal of Fluids Engineering*, 100(2), 215-223.

Francis, R, Ebenezer, DD, Bhattacharyya, SK, and Sharma, R (2023). "Estimation of wavenumber–frequency spectra of wall pressure due to turbulent flow over a flat plate using large-eddy simulation," *Physics of Fluids*, 35(6), 065110.

Hu, Z, Morfey, C and Sandham, D.（2006). "Wall pressure and shear stress spectra from direct simulations of channel flow," *AIAA J*. 44 (7), 1541–1549.

Kim, J (1989). "On the structure of pressure fluctuations in simulated turbulent channel flow," *Journal of Fluid Mechanics*, 205(1), 421.

Kravchenko, AG, Moin, P, and Moser, R (1996). "Zonal Embedded Grids for Numerical Simulations of Wall-Bounded Turbulent Flows," *Journal of Computational Physics*, 127(2), 412–423.

Luo, X, Ye, W, Huang, R, Wang, Y, Du, T, and Huang, C (2020). "Numerical investigations of the energy performance and pressure fluctuations for a waterjet pump in a non-uniform inflow," *Renewable Energy*, 153, 1042–1052.

Park, GI, and Moin, P (2016). "Space-time characteristics of wall-pressure and wall shear-stress fluctuations in wall-modeled large eddy simulation," *Phys Rev Fluids*, 1(2), 024404.

Rezaeiravesh, S, and Liefvendahl, M (2018). "Effect of grid resolution on large eddy simulation of wall-bounded turbulence," *Physics of Fluids*, 30(5), 055106.

Viazzo, S, Dejoan, A, and Schiestel, R (2001). "Spectral features of the wall-pressure fluctuations in turbulent wall flows with and without perturbations using LES," *Int. J. Heat Fluid Flow*, 22, 39–52.

Wang, C, Wang, G, Zhang, M, Huang, B, and Ni, Y-Q (2023). "Wall-pressure fluctuations in attached compressible turbulent cavitating flows," *Phys Rev Fluids*, 8(11), 114301.

Yang, B, and Yang, Z (2022). "On the wavenumber–frequency spectrum of the wall pressure fluctuations in turbulent channel flow," *Journal of Fluid Mechanics*, 937, A39.

Yang, X, and Griffin, KP (2021). "Grid-point and time-step requirements for direct numerical simulation and large-eddy simulation," *Physics of Fluids*, 33(1), 01510.